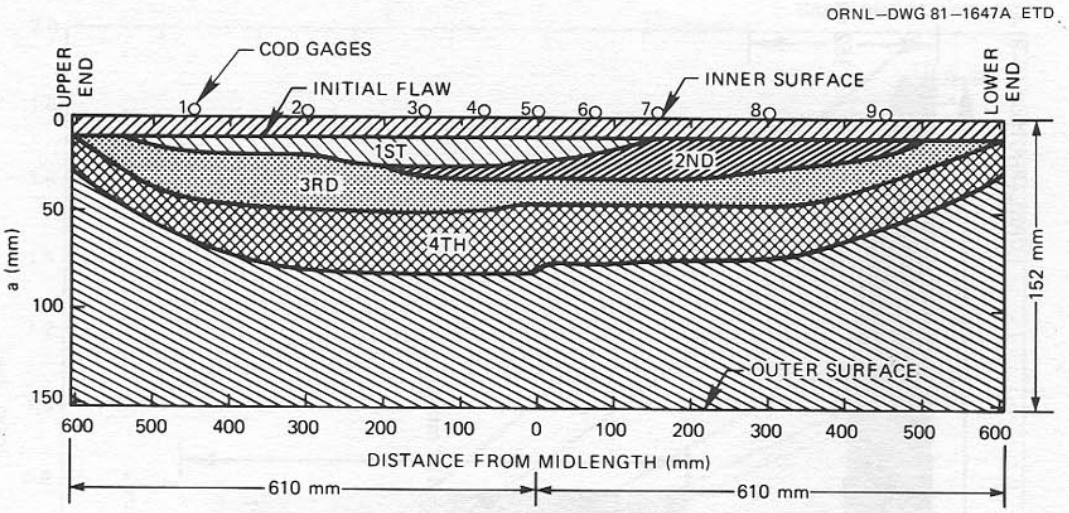

Fig. 9.9. Schematic cross section of TSE-5A test-cylinder wall, showing four-step progression of long axial flaw as deduced from fracture surfaces.

shortly thereafter. A composite photograph of the entire fracture surface is shown in Fig. 9.10 along with an enlarged view of one section. Figure 9.9 was constructed by obtaining measurements of crack depth from photographs of this type.

Figure 9.10 shows a clear indication of an additional event just ahead of the final arrest event. This event was not detected with the COD gages but, rather with the UT instrumentation, as were the four major events. According to an analysis of the UT data, the time between the final arrest event and the preceding arrest event was only 900 μs. This short period of time suggests that the additional event was the result of dynamic effects that created an oscillation in K_I. When K_I dipped down, arrest took place, but immediately thereafter initiation took place as K_I increased. Such oscillations have been observed in lab K_{Ia} tests,[1] and dynamic analyses of the lab specimens indicate such behavior.[2] A dynamic analysis was also attempted for TSE-5A; it did not indicate that a momentary arrest event would take place.[3]

9.3 Crack Depths

Crack depths were determined from the COD and UT data and also from direct observations of the fracture surfaces. The COD data were analyzed in the manner described in Sect. 8.5, and the calculated relation between COD and crack depth for times of interest during TSE-5A is shown in Fig. 9.11. Crack depths based on COD and UT data and obtained from examination of the fracture surfaces are presented in Table 9.1 for the central portion of the test cylinder. As indicated, the agreement is reasonably good.

Table 9.1. Estimated crack depths near midlength of test cylinder for TSE-5A

Event No.	Event	Time (s)	Crack depth (mm)		
			COD	Fracture surface	UT
1	Initiation	78.5	12	12	11
	Arrest		21	23	17
2	Arrest	90.5	30	30	31
3	Arrest	123.0	48	48	41
4	Arrest	184.5	81	81	81

9.4 Fracture-Mechanics Analysis

9.4.1 Posttest analysis based on design toughness curves

The number of initiation-arrest events taking place during TSE-5A agrees with the pretest analysis (Fig. 4.8), but the times at which the events actually took place were earlier than calculated. This indicated that the thermal shock was more severe than that used for the pretest analysis and/or that the actual material toughness was less than that used in the pretest analysis. As planned (Fig. 9.1), the thermal shock was more severe than that assumed for the pretest analysis (that achieved during TSE-5), and, apparently, the toughness was less than assumed, as discussed below.

The toughness curves used in the pretest analysis are shown in Fig. 9.13. The K_{Ic} curve represents the lower bound of fifty 1T-CS data points, while the K_{Ia} curve is a mean curve through six data points obtained from 25 × 151 × 151-mm, wedge-loaded, crack-arrest specimens (also refer to Fig. 7.11).

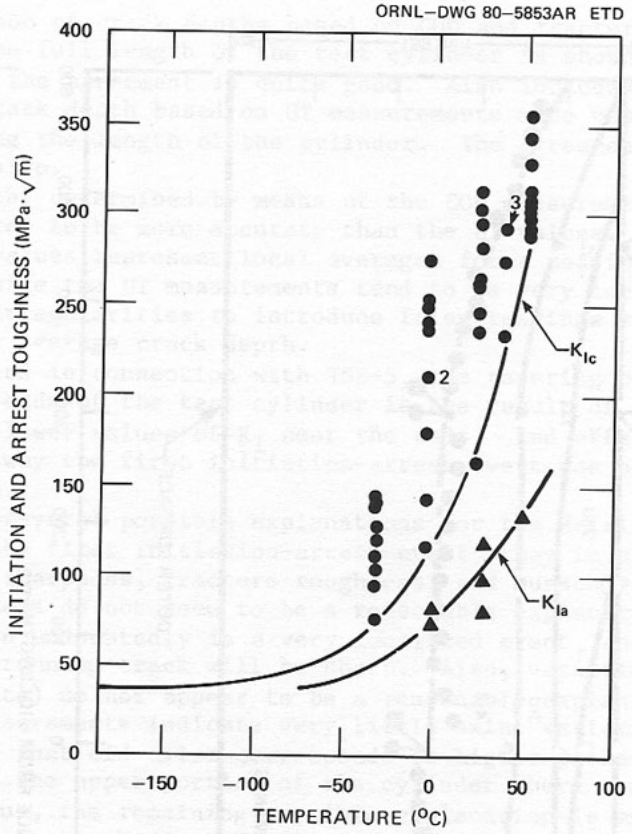

Fig. 9.13. Lower-bound K_J and mean K_{Ia} curves (based on pretest lab data only) used for K_{Ic} and K_{Ia} in TSE-5A pretest analysis.

Posttest analyses of TSE-5A were conducted using the measured test-cylinder temperatures shown in Figs. 9.2–9.6. The results of such an analysis, based on the toughness curves in Fig. 9.13, are shown in Fig. 9.14, which is a set of critical-crack-depth curves that includes the actual path of events. It is observed that the initiation and arrest events fall to the left of their respective initiation and arrest curves, indicating that the actual crack-initiation and crack-arrest toughness values were below the curves in Fig. 9.13.

9.4.2 K_{Ic} and K_{Ia} values deduced from TSE-5A

Critical values of K_I corresponding to the four initiation and arrest events during TSE-5A are shown in Table 9.2, and these values are compared with the experiment-design toughness curves in Fig. 9.15. It is obvious that the K_{Ic} and K_{Ia} values deduced from TSE-5A are substantially less than the values assumed for the design of the experiment on the bases of the lab data. Of course, this was to be expected insofar as crack initiation is concerned because none of the lab initiation data

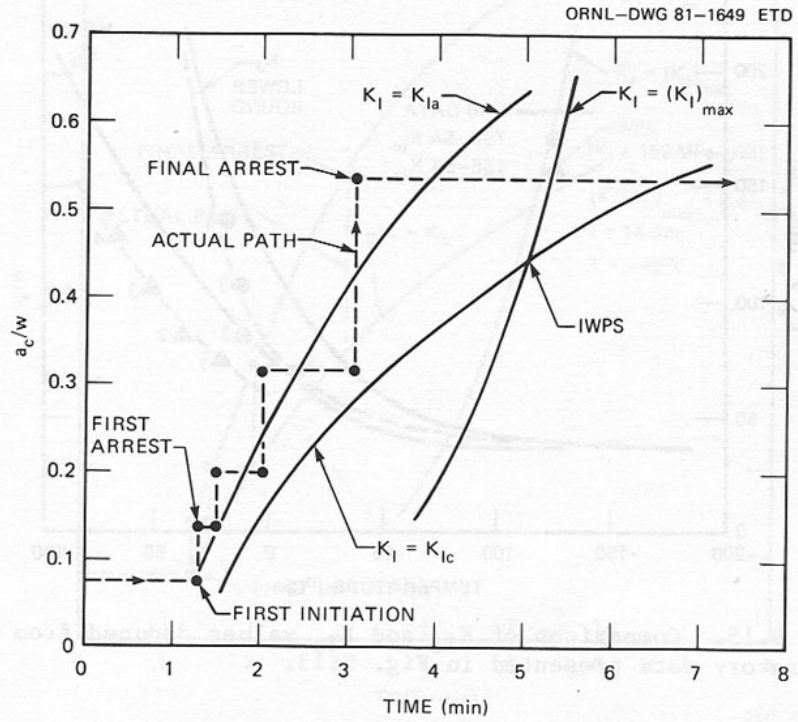

Fig. 9.14. Critical-crack-depth curves for TSE-5A based on toughness curves in Fig. 9.13.

Table 9.2. Summary of critical data for TSE-5A

Time (s)	Event	a/w	K_I (MPa•$\sqrt{m}$)	Temperature (°C)
78.5	1st initiation	0.076	70	−11
90.5	2nd initiation	0.138	85	12
123.0	3rd initiation	0.198	108	13
184.5	4th initiation	0.316	135	21
78.5	1st arrest	0.138	76	22
90.5	2nd arrest	0.198	86	38
123.0	3rd arrest	0.316	107	51
184.5[a]	4th arrest	0.535	130	67

[a] K_I/K_{Ic} reached a maximum value of 2.3 at ~14 min.

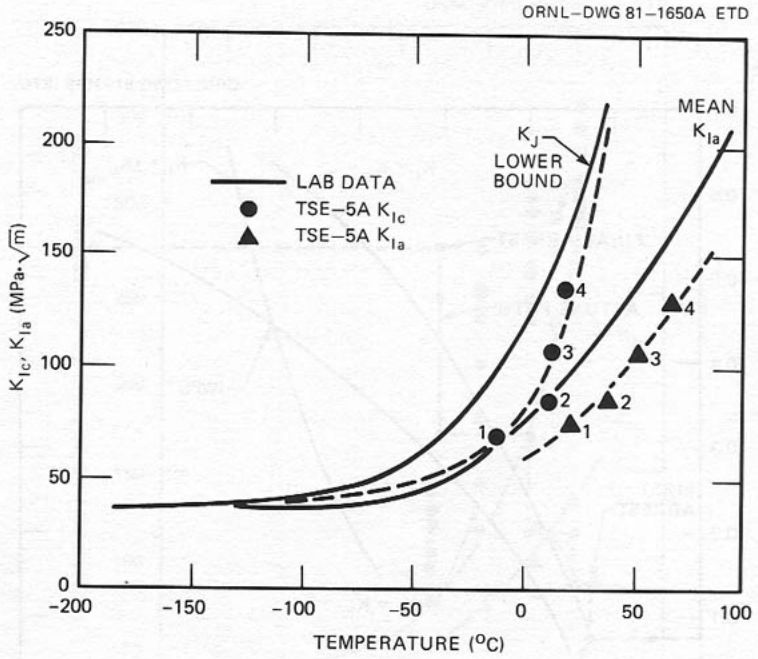

Fig. 9.15. Comparison of K_{Ic} and K_{Ia} values deduced from TSE-5A with laboratory data presented in Fig. 9.13.

points was valid. However, as indicated below, the lab data were adequate for designing the experiment; that is, all objectives of TSE-5A were achieved.

9.4.3 Posttest analysis based on K_{Ic} and K_{Ia} curves deduced from TSE-5A

The dashed curves in Fig. 9.15 represent a best fit of the K_{Ic} and K_{Ia} data points deduced from TSE-5A. These curves were used in a second posttest analysis, and as one would expect, the agreement between actual and "predicted" flaw behavior is much better than when using the solid curves in Fig. 9.15. Results of the second posttest analysis are shown in Fig. 9.16, and a complete set of digital output is included in Appendix E.

9.4.4 Warm prestressing

Figure 9.16 indicates that a fifth crack-initiation event was prevented by warm prestressing, and the maximum value of K_I/K_{Ic} for the final crack depth was 2.3. This maximum value was reached ~9 min after the time of incipient warm prestressing, and the corresponding crack-tip

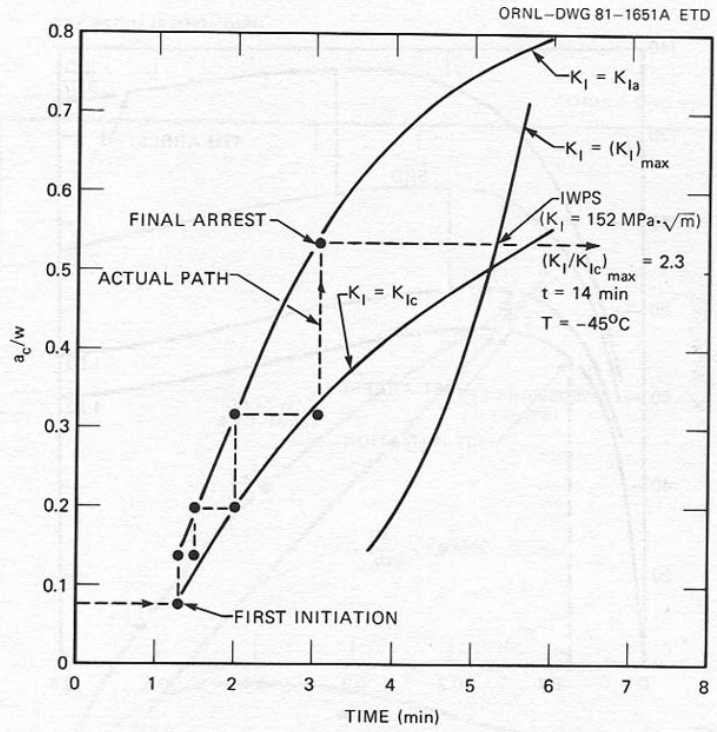

Fig. 9.16. Posttest critical-crack-depth curves for TSE-5A using modified toughness curves in Fig. 9.15.

temperature was −45°C (RTNDT = 10°C). The maximum value of K_I for the final crack depth was 152 MPa•√m, and, of course, it occurred at the time of incipient warm prestressing (~5 min).

The value of 2.3 for $(K_I/K_{Ic})_{max}$ is large enough, relative to unity, to compensate for all uncertainties in the experiment and related post-test analysis, and the crack-tip temperature corresponding to this value was well below RTNDT. Thus, even though the value of $(K_I)_{max}$ for the final crack depth was substantially less than that predicted for the PWR LBLOCA, TSE-5A provided a convincing demonstration of the ability of warm prestressing to prevent crack initiation.

2.4.3. TSE-6

The TSE-6 cylinder had a thinner wall (76 mm vs. 152 mm for the other tests) and introduced the potential for a single long crack jump to a depth greater than 90% of the wall thickness. There were actually two crack jumps in the test. The first was relatively short, and the total penetration was 93% of the wall thickness. One contributor to the difference between pretest analyses and test results is that the specimen toughness was somewhat lower than initially assumed. The test results and posttest analyses are discussed in the following pages taken from (Cheverton 85a). In addition to helping demonstrate the predictability of fracture behavior under thermal shock conditions, TSE-6 helped demonstrate the inability of a long flaw to fully penetrate the vessel wall under thermal shock only loads.

10.2 Events During TSE-6

As indicated in Fig. 10.4, which shows the final profile of the flaw near midlength of the test cylinder, the TSE-6 flaw penetrated very deep (>90%) into the wall of the test cylinder but did not extend all the way through, consistent with predictions. The COD data and a photograph of the full length of the fracture surface (Fig. 10.5) indicate that there were three initiation-arrest events involved. Two of these events, the first and last, were detected with COD gages that were connected to "slow" recorders, and the recorded output of the gages is shown in Fig. 10.6. The second event was detected with two COD gages that were connected to a fast-phenomena recorder, and the output for one of these gages is shown in Fig. 10.7. It is apparent that the second arrest event was the result of a momentary decrease in K_I because ~300 μs thereafter the third initiation-arrest event took place, presumably the result of a momentary increase in K_I (the time between arrest events was ~900 μs, the same as for TSE-5A). A dynamic analysis similar to that performed for TSE-5A was also attempted for TSE-6 (Sect. 9.2). This time the analysis indicated that the momentary arrest event would take place.[1]

The TSE-6 dynamic event appears to be the same type of dynamic event that took place during TSE-5A, and it is of interest to note that in TSE-5A the crack jump preceding the short duration of the arrest event was much shorter and the vessel wall was much stiffer. Thus, it is not clear

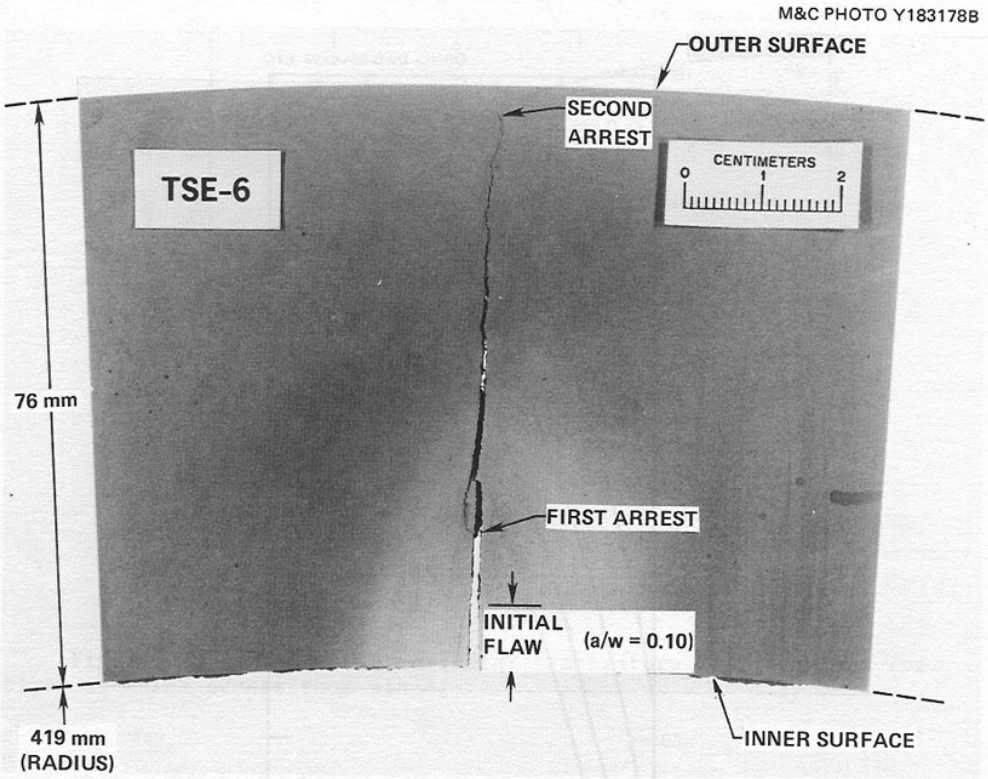

Fig. 10.4. Final radial profile of TSE-6 flaw near midlength of test cylinder.

that the longer crack jump and the less-stiff wall associated with TSE-6 contributed to this particular dynamic effect, which was a point of concern prior to TSE-6.

10.3 Crack Depths

As shown in Fig. 10.5, the initial flaw was uniform in depth (a/w = 0.10) and extended the full length of the test cylinder. Even so, the crack front associated with the first arrest event did not extend all the way to the ends, and the depth of the arrested front is somewhat less at midlength than elsewhere. Ignoring the tapering off at the ends of the flaw, the fractional depth (a/w) of the first arrested crack front varies from 0.21 to 0.32, and there is a 240-mm length in the lower half of the cylinder that has a uniform value of 0.28. With the exception of the tapering off at the ends, which is due to free-end effects, the variation of crack depth is probably due to small axial variations in fracture toughness.

The final crack depth was uniform over ~75% of the length of the test cylinder and was equal to 93% of the wall thickness (a/w = 0.93). At the ends of the cylinder, a/w = 0.82.

The crack depth associated with the very brief second arrest event was ~82% of the wall thickness (a/w = 0.82). Thus, this brief arrest event took place rather close to the site of the final arrest event, as was the case with TSE-5A.

10.4 Fracture-Mechanics Analysis

10.4.1 Posttest analysis based on design toughness curves

The pretest analysis for TSE-6 was based on toughness curves (TSE-6 design curves) deduced from the results of TSE-5 and indicated that only one initiation-arrest event would take place (see Fig. 4.9). Furthermore, a posttest analysis, based on actual temperatures and the design toughness curves, also indicates a single initiation-arrest event, as shown in Fig. 10.8. However, as discussed in Sect. 10.2, there were actually two "static" events and one "dynamic" event. As shown in Fig. 10.8, which includes the actual path of events, the first initiation-arrest event took place ~44 s earlier than "predicted," indicating that the actual fracture toughness was less than anticipated.

A quantitative comparison of K_{Ic} and K_{Ia} data can be obtained using Figs. 10.9 and 10.10, which correspond to Fig. 10.8 and are plots of T, K_I, K_{Ic}, and K_{Ia} vs a/w for the two times when events took place. These figures show that K_{Ic} and K_{Ia} for the first initiation-arrest event were ~40 and ~14% less, respectively, than the design values. For the second initiation and final arrest event, K_{Ic} and K_{Ia} were somewhat greater (24 and 18%, respectively) than the design values.

10.4.2. K_{Ic} and K_{Ia} values deduced from TSE-6

The calculated critical values of K_I corresponding to the first two initiation events and the first and last arrest events are listed in Table 10.1, which also includes for these events the times, crack depths, and crack-tip temperatures. These critical values of K_I are compared with the TSE-6 design curves and the lab small-specimen data in Fig. 10.11. As indicated in this figure, the values of K_{Ic} and K_{Ia} deduced from TSE-6 agree reasonably well with the curves corresponding to the final set of small-specimen data, although the K_{Ic} and K_{Ia} values corresponding to the second initiation event and the final arrest event seem somewhat high.

10.4.3 Posttest analysis based on final set of lab small-specimen K_J and K_{Ia} data

The few TSE-6 data points in Table 10.1 and Fig. 10.11 could not be used in a meaningful way to construct K_{Ic} and K_{Ia} curves for a final posttest analysis of TSE-6. Instead, a final analysis was performed

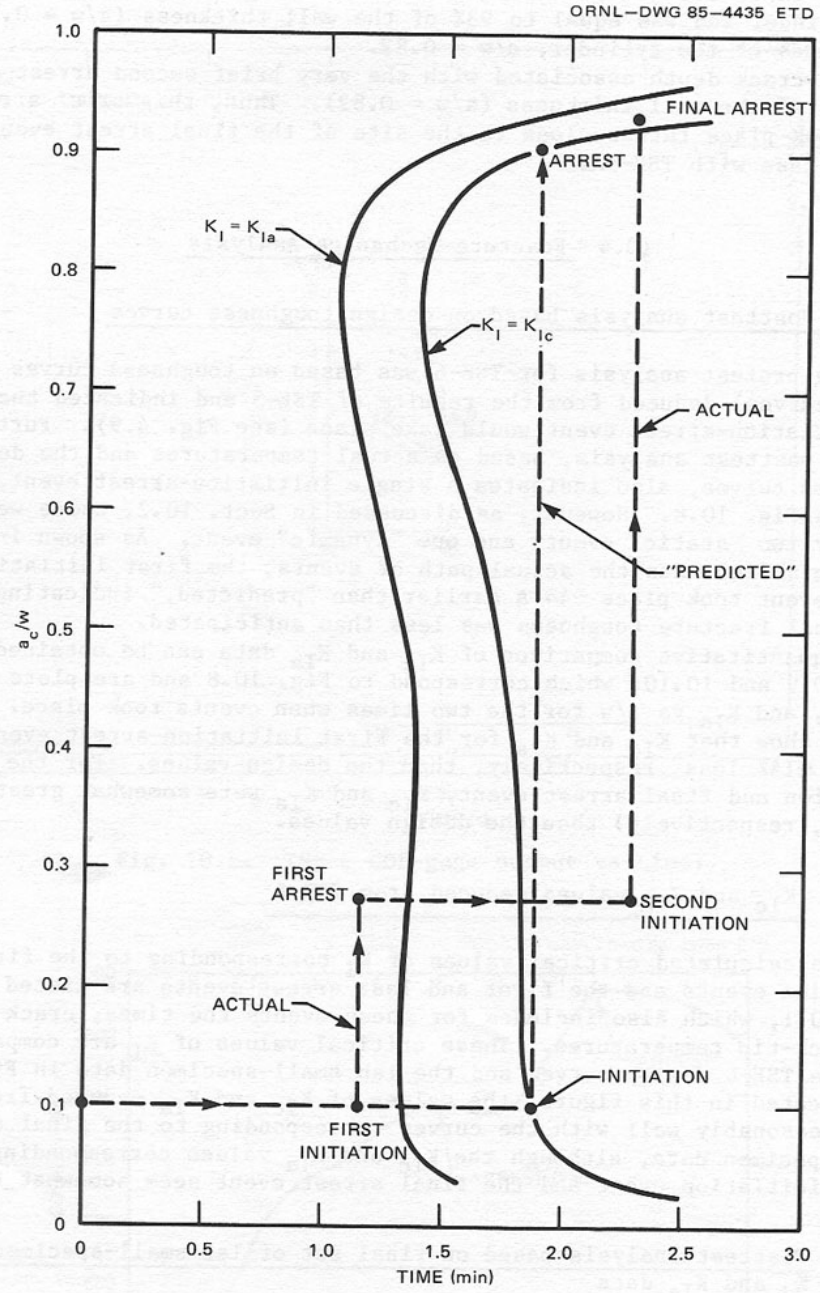

Fig. 10.8. TSE-6 posttest critical-crack-depth curves, based on measured temperatures and design toughness curves, with actual events superimposed.

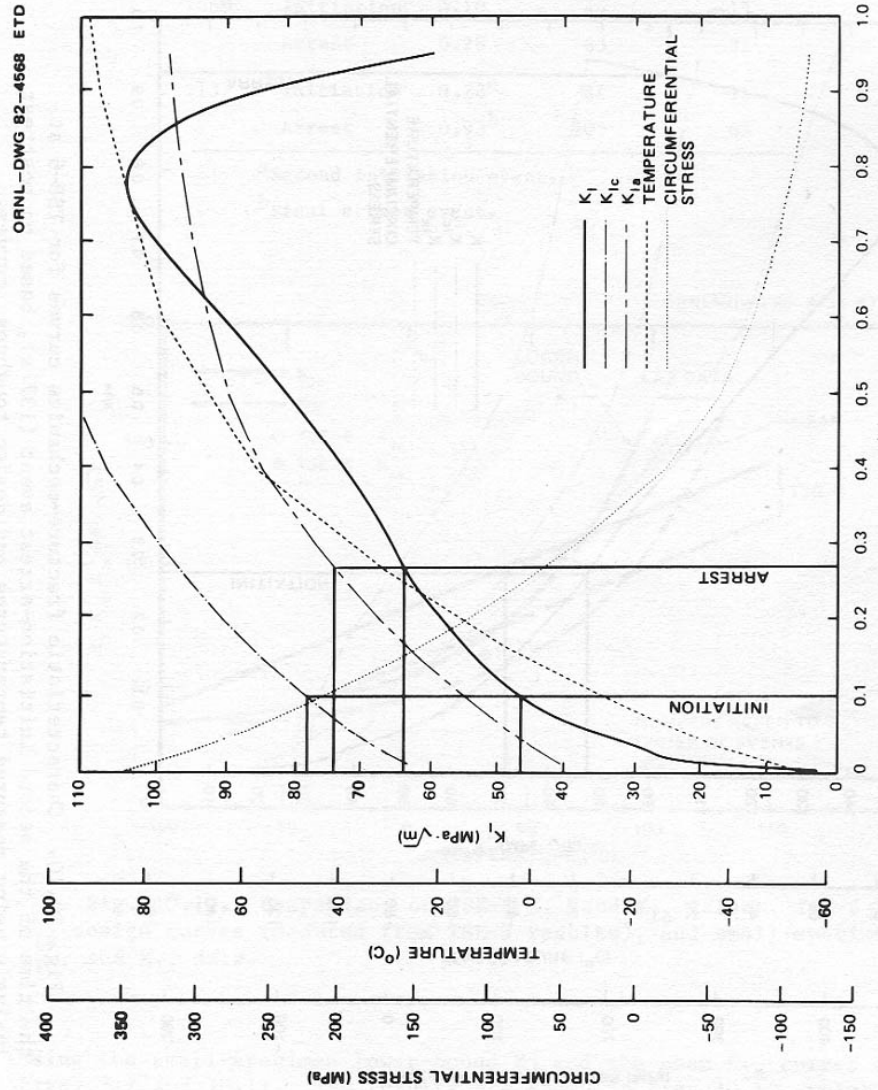

Fig. 10.9. Characteristic fracture-mechanics curves for TSE-6 at the time of the first initiation-arrest event (69 s), based on posttest analysis using measured temperatures and design toughness curves.

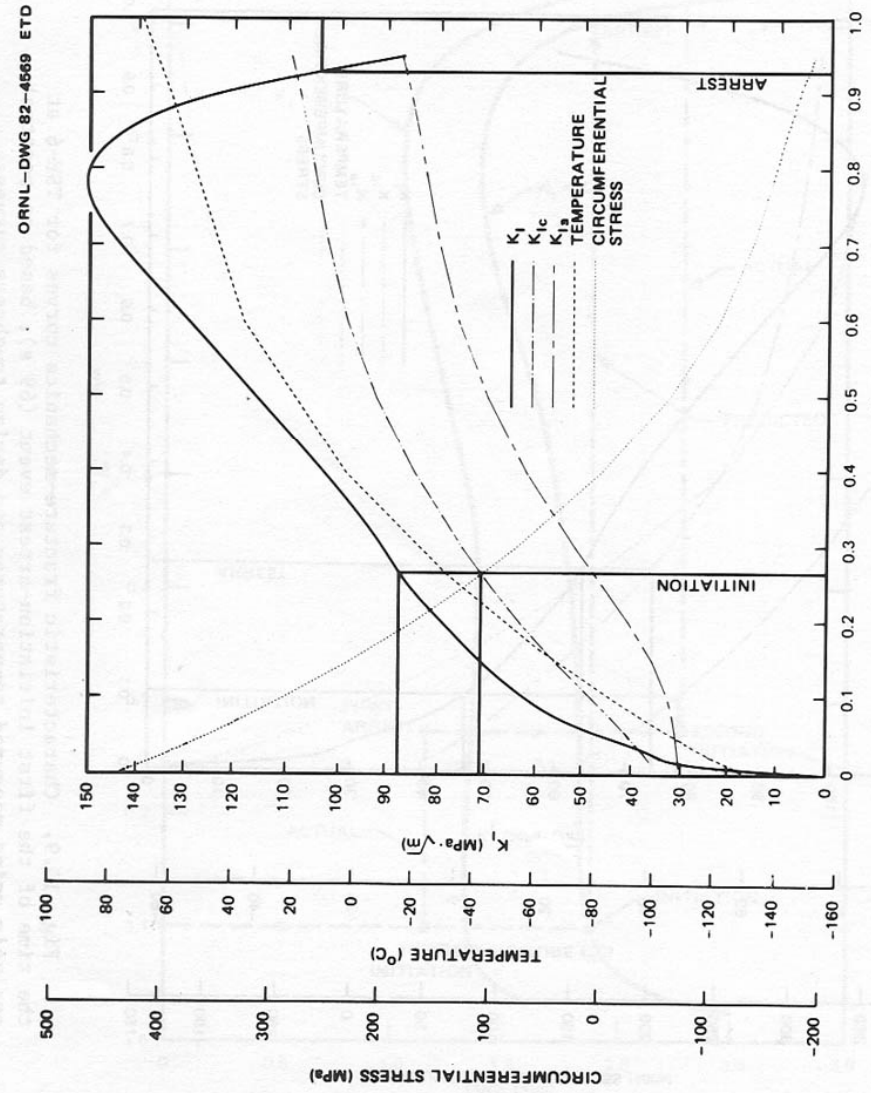

Fig. 10.10. Characteristic fracture-mechanics curves for TSE-6 at the time of the second initiation-arrest event (137 s), based on posttest analysis using measured temperatures and design toughness curves.

Table 10.1. Summary of events for TSE-6

Time (s)	Event	a/w	K_I (MPa•√m)	Temperature (°C)
69	Initiation	0.10	46	−13
	Arrest	0.28	63	32
137	Initiation	0.28[a]	87	−31
	Arrest	0.93[b]	105	63

[a]Second initiation event.

[b]Final arrest event.

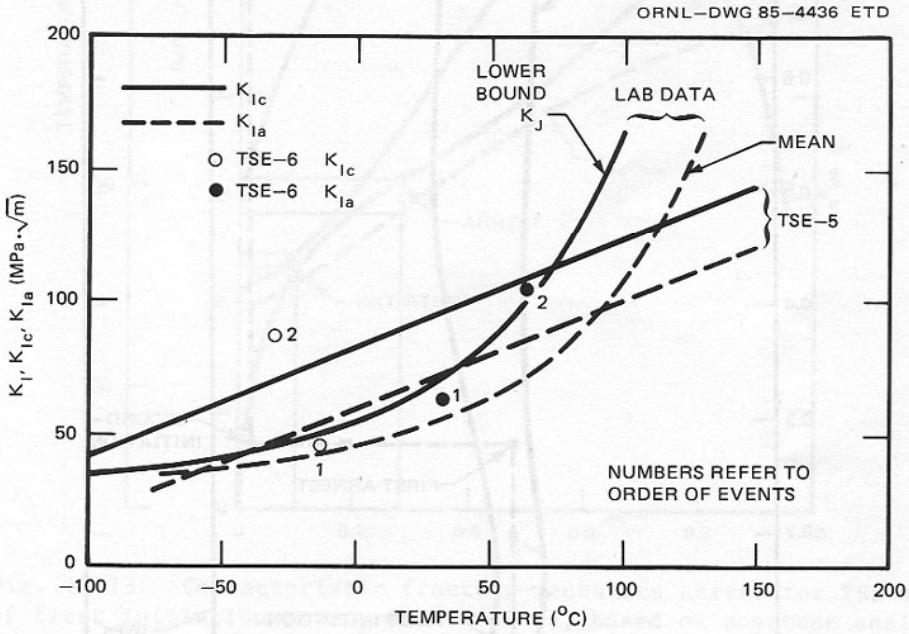

Fig. 10.11. Comparison of TSE-6 K_{Ic} and K_{Ia} values, TSE-6 K_{Ic} and K_{Ia} design curves (deduced from TSE-5 results), and small-specimen K_J, K_{Ic}, and K_{Ia} data.

using the small-specimen lower-bound K_J and the mean K_{Ia} curves shown in Figs. 7.7 and 10.11. The results are shown in Fig. 10.12, which is a set of critical-crack-depth curves with the actual events superimposed, and in Figs. 10.13 and 10.14, which are plots of temperature, K_I, K_{Ic} and K_{Ia} vs a/w for the two times at which events took place. (A complete set of digital output is included in Appendix F.) These results indicate reasonably good agreement between experiment and analysis for the first

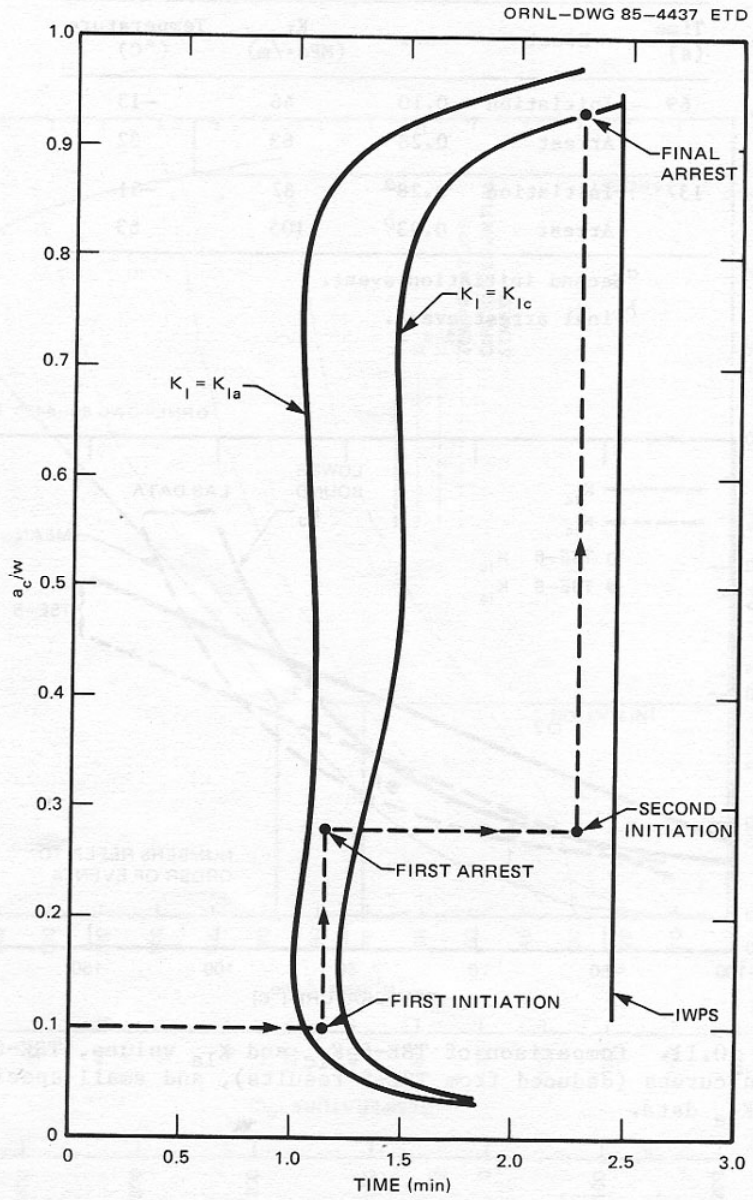

Fig. 10.12. TSE-6 posttest critical-crack-depth curves, based on measured temperatures and lab small-specimen lower-bound K_J and mean K_{Ia} data, with actual events superimposed.

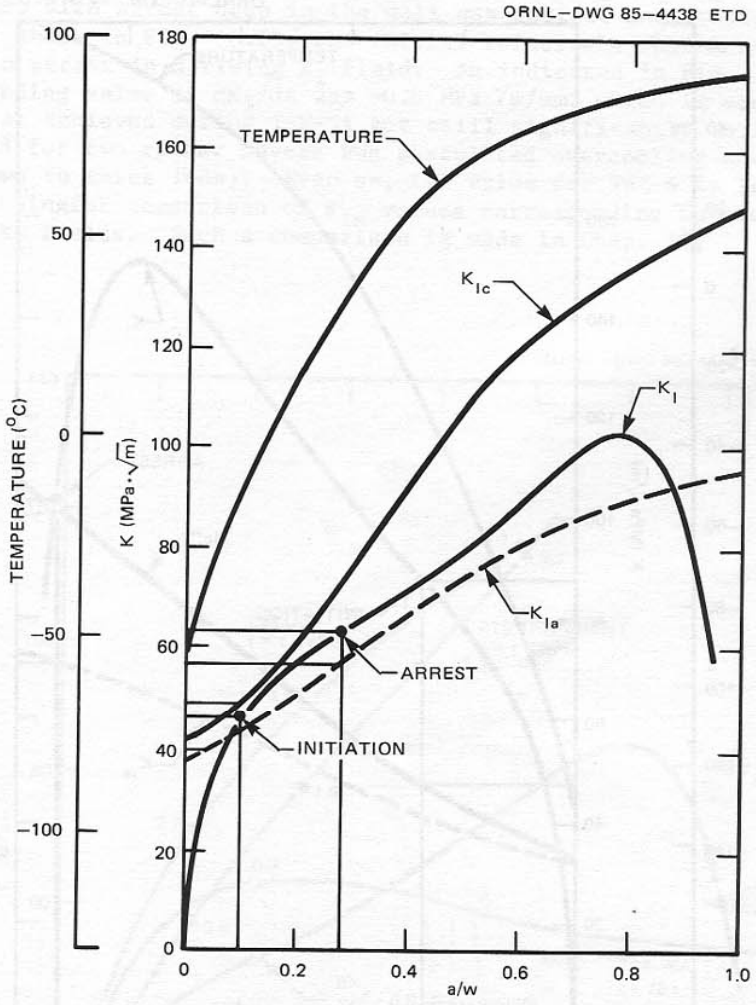

Fig. 10.13. Characteristic fracture-mechanics curves for TSE-6 at time of first initiation-arrest event (69 s), based on posttest analysis using small-specimen fracture-toughness data.

initiation, first arrest, and final arrest event and a rather large discrepancy for the second initiation event, consistent with the data in Fig. 10.11. The critical values of K_I corresponding to the first initiation and arrest events are ~6% less and ~12% greater, respectively, than the corresponding toughness curves. For the second initiation event, the critical value of K_I is ~88% greater than the initiation toughness curve.

A comparison of K_I and K_{Ia} for the final arrest event may not be very meaningful because of the proximity of the crack tip to the outer surface of the cylinder and because of the apparent very steep gradient in K_I, which makes the calculated critical value of K_I very sensitive to the effective crack depth. Probably the most important observation is

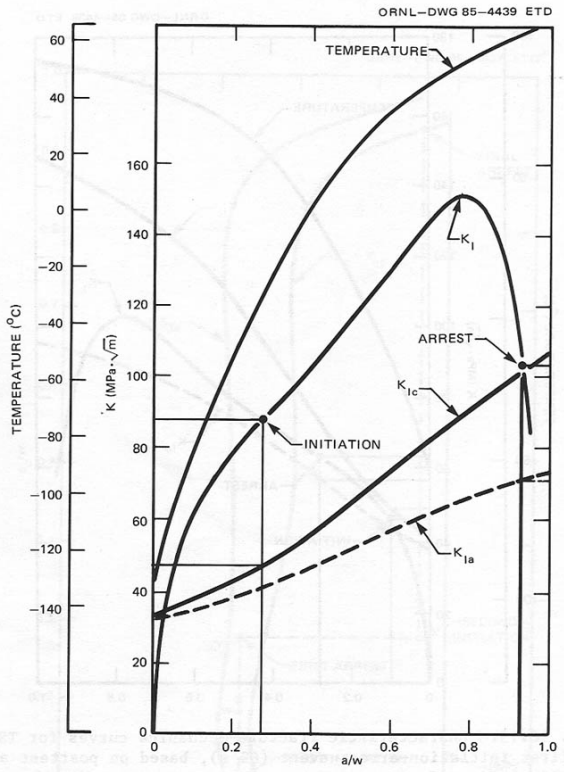

Fig. 10.14. Characteristic fracture-mechanics curves for TSE-6 at time of second initiation-arrest event (137 s), based on posttest analysis using small-specimen fracture-toughness data.

that almost irrespective of the value of K_{Ia}, the calculation would predict arrest deep in the wall (a/w > 0.9) and, indeed, that is what happened.

2.4.4. Crack Initiation and Arrest Values from TSE-5, 5A, and 6

(Cheverton 85a and 86) compared the critical values of K_I corresponding to crack initiation and arrest events with laboratory specimen data (Figs. 3 and 4 below).

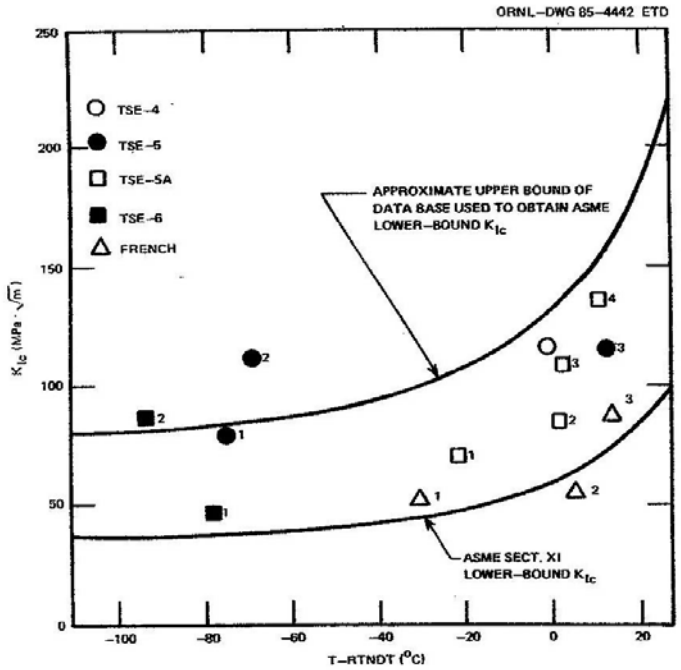

Fig. 3. Comparison of K_{Ic} data from TSE cylinder tests and laboratory specimens.

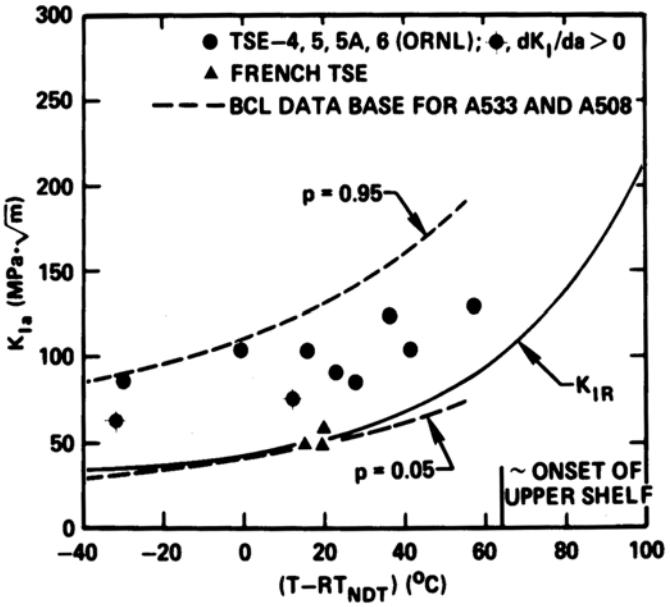

Fig. 4. Comparison of K_{Ia} data from TSE cylinder tests and laboratory specimens.

The curves shown in these figures are the upper- and lower-bound curves from small-specimen data. Overall, the K_{Ic} and K_{Ia} values derived from these TSE experiments demonstrate that the fracture behavior under these large-scale thermal-shock situations are adequately predicted by the use of LEFM methods and fracture properties obtained from tests of small laboratory specimens.

3. Summary Discussion

The discussion in this Appendix has shown that multiple flaw initiation-arrest events are credible for thick-wall cylinders exposed to thermal-shock transients. Additionally, it has shown that the nature and extent of such fracture behavior can be adequately predicted by careful application of linear elastic fracture mechanics analyses. This discussion has centered on the series of Thermal-Shock Experiments that was conducted within the HSST program at ORNL. Because the basic factors driving the fracture behavior in these TSEs are so similar to those for PTS scenarios, multiple fracture run-arrest events are deemed credible for an RPV exposed to PTS transient loads.